

Anisotropic spin waves and exchange interactions in the *A*-type antiferromagnetic state of $\text{Pr}_{0.5}\text{Sr}_{0.5}\text{MnO}_3$

V. V. Krishnamurthy,¹ J. L. Robertson,¹ R. S. Fishman,¹ M. D. Lumsden,¹ and J. F. Mitchell²

¹*Condensed Matter Sciences Division, Oak Ridge National Laboratory, Oak Ridge, Tennessee 37831-6430, USA*

²*Materials Science Division, Argonne National Laboratory, Argonne, Illinois 60439, USA*

(Received 12 September 2005; revised manuscript received 20 January 2006; published 16 February 2006)

Inelastic neutron scattering is used to investigate the spin dynamics in the layered *A*-type antiferromagnetic state of $\text{Pr}_{0.5}\text{Sr}_{0.5}\text{MnO}_3$ at 20 K. The spin wave dispersion, observed between 2 and 12 meV, for neutron momentum transfer, \mathbf{Q} , parallel to the ferromagnetic planes is found to be much steeper than the dispersion when \mathbf{Q} is perpendicular to the ferromagnetic planes, indicating strong anisotropy. Here we show that the three-dimensional Heisenberg model with nearest neighbor exchange interactions, an interlayer antiferromagnetic coupling, an intralayer ferromagnetic coupling, and a single ion anisotropy can account for these dispersions. A comparison of the ratio of exchange couplings in $\text{Pr}_{0.5}\text{Sr}_{0.5}\text{MnO}_3$ and LaMnO_3 shows that the anisotropy of exchange interactions strongly depends on the type of orbital ordering.

DOI: [10.1103/PhysRevB.73.060404](https://doi.org/10.1103/PhysRevB.73.060404)

PACS number(s): 75.47.Lx, 75.30.Ds., 75.47.Gk, 78.70.Nx

In complex transition metal oxides, such as cuprates and manganites, magnetism and electrical transport are intricately related. The discovery of superconductivity and colossal magnetoresistance¹⁻³ (CMR) has generated a great deal of interest in transition metal oxides both fundamentally⁴ and technologically.⁵ CMR in half-hole-doped manganites is associated with distinctly different types of electronic conduction in metallic ferromagnetic and insulating antiferromagnetic states; hence it depends on the nature of interatomic exchange interactions. Half-doped manganites as well as several other transition metal oxides exhibit different antiferromagnetic phases, whose magnetic and transport properties are strongly governed by the orbital degrees of freedom in addition to charge and spin degrees of freedom, as has been reported from a large number of experimental and theoretical studies.⁶ Therefore, an understanding of the dependency of interatomic exchange interactions on orbital ordering in the manganites is key to describing a wide range of electronic phenomena in transition metal oxides.

In doped manganites, the hopping of the e_g electrons between Mn^{3+} , which is a Jahn-Teller active ion, and Mn^{4+} ions mediates the double exchange interaction and a ferromagnetic metallic state is realized. In the *A*-type antiferromagnetic state of undoped manganites such as LaMnO_3 , the e_g electrons are localized alternatively in the $d_{3x^2-r^2}$ and $d_{3y^2-r^2}$ orbitals in the *ab* plane. However, in doped manganites, these electrons participate in conduction along specific low-dimensional paths that depend on the magnetic structure. *A*-type antiferromagnetic ordering consists of ferromagnetic layers with antiferromagnetic interlayer coupling. In the case of doped manganites, it is associated with a different type of orbital ordering, i.e., orbital ordering with the $d_{x^2-y^2}$ symmetry. Given the different types of orbital ordering in these two manganites, it is interesting to know if the spin dynamics would be affected. Thus, a detailed knowledge of the spin dynamics, the exchange interactions, and their relation to the spin, lattice, and orbital degrees of freedom in half-doped manganites is required.

$\text{Pr}_{0.5}\text{Sr}_{0.5}\text{MnO}_3$ orders antiferromagnetically in the layered

A-type structure (Néel temperature $T_N=140$ K), rather than in the typical charge exchange (CE)-type zigzag structure.⁷ The antiferromagnetic structure of $\text{Pr}_{0.5}\text{Sr}_{0.5}\text{MnO}_3$ consists of a ferromagnetic order within the planes of Mn atoms perpendicular to the (101) direction and antiferromagnetic coupling between the planes, i.e., along the (101) direction. Electrical resistivity measurements suggest semiconducting behavior in the antiferromagnetic state.⁷ The optical conductivity, for the case of the electric field parallel to the ferromagnetic planes, shows pseudogaps with peaks at 0.5 eV.⁸ Here we report the results of a neutron scattering investigation of the excitations in the antiferromagnetic state of $\text{Pr}_{0.5}\text{Sr}_{0.5}\text{MnO}_3$. Highly anisotropic spin waves from the Mn sublattice are observed in the energy range from 2 to 12 meV. These results enable us to understand the nature of the coupling between the magnetic moments in a layered structure and the role played by the orbitals in the spin dynamics.

A single crystal of $\text{Pr}_{0.5}\text{Sr}_{0.5}\text{MnO}_3$ weighing 2.5 g, with a diameter of 5 mm and a length of 25 mm, was grown by the floating zone method. Inelastic neutron scattering experiments were performed using the HB3 triple-axis spectrometer at the High Flux Isotope Reactor, Oak Ridge National Laboratory. A PG(002) monochromator and a PG(002) analyzer were used with the final energy of the analyzer E_f fixed at 13.7 meV and the collimation of 120'-40'-40'-120' was used. The energy transfer explored in this investigation ranged from 2 to 25 meV. The majority of the data was collected within the *HOL* scattering plane, corresponding to the *ac* plane in real space, by holding the energy transfer constant (energy loss is positive by convention) and scanning the neutron momentum transfer perpendicular to the ferromagnetic planes $(0.5, 0, 0.5) < \mathbf{Q} < (2, 0, 2)$ in one case and parallel to the ferromagnetic planes $(2, 0, 1) < \mathbf{Q} < (1, 0, 2)$ in the other.

Figure 1(a) shows the observed neutron inelastic scattering intensity for neutron energy transfer from 2 to 22 meV and neutron momentum transfer perpendicular to the ferromagnetic planes while Fig. 1(b) shows the intensity parallel to the ferromagnetic planes. These intensity plots map out

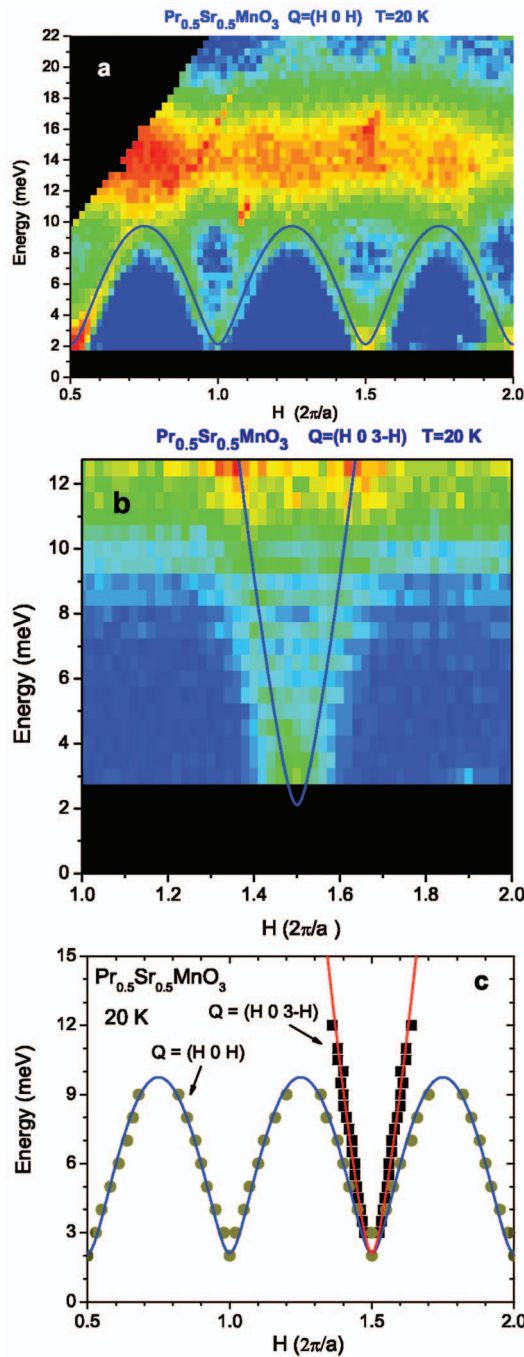


FIG. 1. (Color) (a) Inelastic neutron scattering intensity map in the antiferromagnetic state of $\text{Pr}_{0.5}\text{Sr}_{0.5}\text{MnO}_3$ measured along $\mathbf{Q} = (H 0 H)$ (perpendicular to the ferromagnetic planes) at 20 K. The solid line is the dispersion given by Eq. (4). (b) The spin wave dispersion for \mathbf{Q} along the $[H 0 3-H]$ directions (parallel to the ferromagnetic planes). The solid line is the dispersion given by Eq. (5). Crystal field excitations of Pr ions are present at about 12.8 and 15.35 meV. (c) Magnon peak energies showing the spin wave dispersion for \mathbf{Q} along $(H 0 H)$ (circles) and for \mathbf{Q} along $(H 0 3-H)$ (squares) along with the fits by Eqs. (4) and (5). The error bars are of the size of the symbols.

the dispersion of the magnetic excitations from antiferromagnetic spin waves on the Mn sublattice in the 2–12 meV range and are directly related to the dynamic structure factor

$S(\mathbf{Q}, \omega)$. Here, ω is the frequency of the magnon excitations and is related to the neutron energy transfer by $E = \hbar\omega$. The dispersion shows a strong oscillatory pattern in both directions and is consistent with one spin wave branch from the Mn sublattice with the minima both at the ferromagnetic zone center and at the antiferromagnetic zone center. Figure 1(c) shows the result of fitting the intensity profiles with a model of the structure factor as described below. The anisotropy between the two spin directions is clearly evident. The energy gap in the dispersion at the zone center has been measured, also at 20 K, in another experiment performed on a cold neutron triple-axis spectrometer RITA-2 at the swiss spallation neutron source (SINQ), and was found to be 2.07 ± 0.1 meV.⁹ Figure 1(a) also shows a very strong intensity at higher energy between 12 and 20 meV which is nearly independent of Q . Constant Q scans as a function of temperature between 20 and 250 K confirm that the excitations in the 12–20 meV region originate from the crystalline electric field (CEF) excitations of the Pr ions.

To understand the excitations of Mn ions, we consider the Mn–Mn interatomic distances and the possible paths for exchange interactions among Mn ions. The nearest neighbor (3.754 Å) Mn–Mn coupling is the antiferromagnetic superexchange interaction J_a mediated by the oxygen ions along the (101) direction. Both the second nearest neighbor (3.841 Å) and the third nearest neighbor (3.914 Å) Mn–Mn couplings are ferromagnetic exchange interactions. To explain the spin wave energy spectrum of $\text{Pr}_{0.5}\text{Sr}_{0.5}\text{MnO}_3$, we consider an effective three-dimensional (3D) Heisenberg model as in Ref. 10, but with an additional single-ion anisotropy term to account for the observed energy gap:

$$H = -J_f \sum_{ij \parallel \text{planes}} \mathbf{S}_i \cdot \mathbf{S}_j + J_a \sum_{ij \perp \text{planes}} \mathbf{S}_i \cdot \mathbf{S}_j - (D/2) \sum_i S_{iz}^2, \quad (1)$$

where J_f is the ferromagnetic coupling within the planes, J_a is the antiferromagnetic coupling between the ferromagnetic planes, and D is the single-ion anisotropy energy. The solution of the Hamiltonian by the $1/S$ expansion method yielded the spin wave dispersion:

$$\hbar\omega(\mathbf{Q}) = 2S \left\{ 2J_f [1 - \gamma_+(\mathbf{Q})] + J_a + D/2 \right\}^2 - [J_a \gamma_-(\mathbf{Q})]^2 \right\}^{1/2}, \quad (2)$$

where ω ($\hbar\omega$) is the frequency (energy) of the spin wave, S is the effective spin of the Mn, and γ_+ and γ_- are spin wave structure factors.¹¹ To extract the dispersion of the spin waves from the measured inelastic neutron scattering intensity, we have used the structure factor

$$S(\mathbf{Q}, \omega) = \sum_m A_m f_{\text{Mn}}^2(\mathbf{Q}) \frac{\omega_m \Gamma_m [1 + n(\omega_m, T)]}{(\omega - \omega_m)^2 + \Gamma_m^2} + \sum_p B_p f_{\text{Pr}}^2(\mathbf{Q}) \frac{2\Gamma_p}{4\pi(\omega - \omega_p)^2 + \Gamma_p^2}, \quad (3)$$

where the first and second terms correspond to the scattering from the Mn and Pr sublattices, respectively. The index m represents the summation over the magnon excitations of Mn and the index p represents the summation over the crystal field excitations of Pr. In the above equation, A_m and B_p are

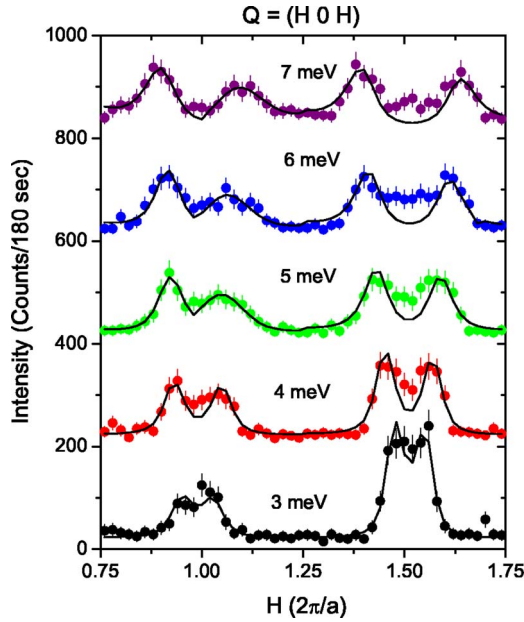


FIG. 2. (Color online) Constant energy scans at 3, 4, 5, 6, and 7 meV for \mathbf{Q} , along $(H 0 H)$ perpendicular to the ferromagnetic planes, measured at 20 K. The solid lines represent best fits by Eq. (3) convoluted with the instrument resolution function. For clarity, spectra at energies 4–7 meV are shifted higher by 200 counts with respect to the adjacent lower energy spectrum.

the scale factors for the magnon and crystal field excitations, respectively. $n(\omega_m) = 1/[1 - \exp(\hbar\omega_m/k_B T)]$ is the Bose temperature factor, f_{Mn} is the averaged magnetic form factor for Mn^{3+} and Mn^{4+} , f_{Pr} is the magnetic form factor for Pr^{3+} , ω_m are the spin wave frequencies, Γ_m are the full width at half maximum of the magnon peaks, ω_p are the frequencies (centroids) of the Pr CEF excitations (Lorentzians), and Γ_p are the full width at half maximum of the CEF peaks.

For \mathbf{Q} perpendicular to the ferromagnetic planes, the spin wave dispersion obtained from Eq. (2) is given by

$$\hbar\omega_1 = 2S\sqrt{(J_a + D/2)^2 - [J_a \cos(2\pi H)]^2}. \quad (4)$$

The dispersion for \mathbf{Q} parallel to the ferromagnetic planes is given by

$$\hbar\omega_2 = 2S\sqrt{(J_f[1 - \cos[\pi(2H - 3)]] + J_a + D/2)^2 - J_a^2}. \quad (5)$$

Selected scans with \mathbf{Q} perpendicular to the ferromagnetic planes and the fixed energy transfer are shown in Fig. 2. These scans were fitted¹² by Eq. (3) with the spin wave dispersion given by Eqs. (4) and (5) convoluted with the instrument resolution function derived using the Cooper-Nathans approximation to determine the peak positions. The fits reproduce the peak positions quite accurately at different excitation energies as well as the observed peak widths. The width of the one magnon excitation peak increases with the excitation energy but is nearly independent of Q . The solid lines over the data in Fig. 2 are best fits to Eq. (3) convoluted with the instrumental resolution. The intensities of the magnon peaks for this spin wave branch at different \mathbf{Q} are comparable. Figure 3(a) shows selected constant E scans for \mathbf{Q}

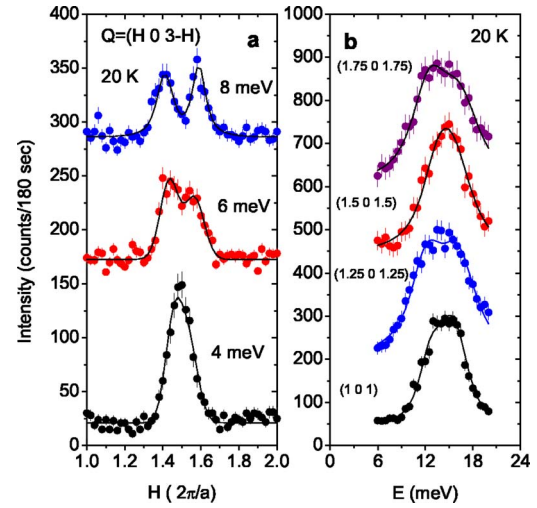


FIG. 3. (a) (Color online) Constant energy scans at 4, 6, and 8 meV for momentum transfer, \mathbf{Q} , along $[H 0 3-H]$ at $T=20$ K. The solid lines are resolution convoluted fits to Eq. (3). (b) Constant Q scans at $Q=[1 0 1]$, $[1.25 0 1.25]$, $[1.5 0 1.5]$, and $[1.75 0 1.75]$ showing two dispersionless excitations of Pr CEF transitions at 20 K. For clarity, the spectra at 6 and 8 meV are shifted higher by 150 and 250 counts, respectively.

parallel to the ferromagnetic planes. For a given energy, the separation between the one magnon peaks in this direction is much less than the separation for \mathbf{Q} perpendicular to the ferromagnetic planes, suggesting a much steeper spin wave dispersion in the parallel direction. In the fitting procedure, we have fixed the value of S to 1.55 based on the magnetic moment $\mu = 2S$ of $3.1\mu_B$ for Mn in the antiferromagnetic state of $Pr_{0.5}Sr_{0.5}MnO_3$.⁷ The solid lines in Fig. 1 for the spin wave branches are the best fits by Eqs. (4) and (5). These fits yield the exchange coupling constants, $J_a = 3.07$ meV, $J_f = 5.83$ meV, and the anisotropy energy $D = 0.15$ meV, indicating that the ferromagnetic coupling is much larger than the antiferromagnetic coupling. The gap in the dispersion $\Delta = 2S[J_a D + D^2/4]^{1/2}$ is 2.11 meV and compares quite well with the value of 2.07 ± 0.1 meV extracted in another experiment using a RITA-2 spectrometer at SINQ.⁹

The above values of J_a and J_f clearly show that the exchange interactions in $Pr_{0.5}Sr_{0.5}MnO_3$ are anisotropic, i.e., ferromagnetic along two directions and antiferromagnetic in the third direction. The origin of anisotropic exchange interactions in $Pr_{0.5}Sr_{0.5}MnO_3$ is most likely associated with $d_{x^2-y^2}$ -type orbital ordering of the e_g electrons in the antiferromagnetic states.^{7,13,14} We note that no Drude peak is observed in the optical conductivity profile of $Pr_{0.5}Sr_{0.5}MnO_3$ in the antiferromagnetic state. Therefore, there is no evidence for metallic behavior in the ferromagnetic planes that is usually expected from the double exchange interaction. The Mn–O–Mn bond angles in the ferromagnetic planes are close to 160° in the monoclinic phase below T_N (Ref. 7) and this favors a ferromagnetic superexchange interaction according to the Goodenough-Kanamori rules.¹⁵ Therefore, we suggest that the ferromagnetic interaction in the planes is mediated by the ferromagnetic superexchange interaction. Thus, we can infer that in two directions of the crystal, the ferromag-

netic superexchange dominates the antiferromagnetic superexchange forming ferromagnetic planes and the antiferromagnetic superexchange couples the ferromagnetic planes in the third direction. The ferromagnetic superexchange interaction together with an in-plane electronic gap or e_g electron localization¹⁶ can explain the semiconducting behavior in the antiferromagnetic state.

The exchange interaction energies in $\text{Pr}_{0.5}\text{Sr}_{0.5}\text{MnO}_3$ are comparable with the values of $J_a=3.3$ meV and $J_f=5.3$ meV in the $\text{Nd}_{0.45}\text{Sr}_{0.55}\text{MnO}_3$ (NSMO) which also has the A-type antiferromagnetic structure, but is more than half-doped.¹⁷ The exchange interactions in $\text{Pr}_{0.5}\text{Sr}_{0.5}\text{MnO}_3$ are larger compared to the values of $J_a=J'=0.6$ meV and $J_f=J=0.83$ meV in the undoped manganite LaMnO_3 in the layered A-type antiferromagnetic state.¹⁸ In the undoped manganite, the localized t_{2g} electrons mediate the antiferromagnetic superexchange interaction. In the half-hole-doped manganites, the e_g electrons mediate both the ferromagnetic and the antiferromagnetic superexchange interactions, thus strongly enhancing their coupling strengths. It is interesting to note that the ratio of exchange interactions J_f/J_a in $\text{Pr}_{0.5}\text{Sr}_{0.5}\text{MnO}_3$ comes out to be 1.9, i.e., much larger than the corresponding ratio of $J/J'=1.38$ in the undoped A-type antiferromagnet LaMnO_3 (Ref. 18), suggesting that the exchange interactions are more anisotropic in the manganite with $d_{x^2-y^2}$ -type orbital ordering. It is likely that this is due to the strong ϕ orbital overlap for e_g states in $d_{x^2-y^2}$ but the small overlaps of $d_{3x^2-r^2}$ and $d_{3y^2-r^2}$ in the z direction. The value of J_f/J_a in the more than half-doped manganite NSMO is 1.6, which is also larger than the ratio found in LaMnO_3 . Therefore, we conclude that the spin dynamics in manganites with A-type antiferromagnetic ordering strongly depends on the type of orbital ordering.

The inelastic neutron scattering intensities in the energy range 12–25 meV show that the excitations in this energy region are dominated by the CEF excitations of Pr ions. Typical scans of the energy transfer $Q=(1,0,1)$ and $(1.5,0,1.5)$ are shown in Fig. 3(b). The best fits of the intensity data by Eq. (3) resulted in the values of 12.8 and 15.35 meV for the two crystal field excitations of Pr ions. The energies of CEF excitations in $\text{Pr}_{0.5}\text{Sr}_{0.5}\text{MnO}_3$ are comparable to those found for Pr in a perovskite compound PrGaO_3 .¹⁹ Pr ions have the C_3 site symmetry in these compounds and similar energy scales of CEF excitations are expected.

In conclusion, inelastic neutron scattering measurements on the layered A-type antiferromagnetic state of the half-hole-doped manganite PSMO show that the spin wave dispersion is anisotropic. An analysis of the dynamic structure factor, using the spin wave dispersion of the 3D Heisenberg model, shows that the ferromagnetic superexchange interaction is larger than the antiferromagnetic superexchange interaction and that the type of orbital ordering plays a role in the spin dynamics. The hole doping, which results in a change in the type of orbital ordering in the A-type antiferromagnetic state in half-doped manganites, enhances the exchange interaction.

We acknowledge helpful discussions with Professor D. Khomskii and Professor T. A. Kaplan. This work was supported by the Oak Ridge National Laboratory, managed by UT-Battelle, LLC, for the US Department of Energy under the Contract No. DE-AC05-00OR22725. The work at Argonne National Laboratory was sponsored by the US Department of Energy, Office of Sciences under the Contract No. W-31-109-ENG-38.

¹S. Jin *et al.*, Science **264**, 413 (1994).

²H. Kuwahara *et al.*, Science **270**, 961 (1995).

³Y. Tomioka, A. Asamitsu, Y. Moritomo, H. Kuwahara, and Y. Tokura, Phys. Rev. Lett. **74**, 5108 (1995).

⁴D. I. Khomskii and G. A. Sawatzky, Solid State Commun. **102**, 87 (1997).

⁵A.-M. Haghiri-Gosnet and J.-P. Renard, J. Phys. D **36**, R127 (2003).

⁶Y. Tokura and N. Nagaosa, Science **288**, 462 (2000).

⁷H. Kawano, R. Kajimoto, H. Yoshizawa, Y. Tomioka, H. Kuwahara, and Y. Tokura, Phys. Rev. Lett. **78**, 4253 (1997).

⁸K. Tobe, T. Kimura, and Y. Tokura, Phys. Rev. B **69**, 014407 (2004).

⁹V. V. Krishnamurthy *et al.* (unpublished).

¹⁰M. Raczowski and A. M. Oles, Phys. Rev. B **66**, 094431 (2002).

¹¹The crystal coordinate system used here is rotated by 45° about the b axis relative to the one used by Krackowski and Oles.¹⁰

When this is taken into account, we get $\gamma_+=1$, $\gamma_-=\cos(2\pi H)$ for \mathbf{Q} perpendicular to the ferromagnetic planes and $\gamma_+=(1/2)[1+\cos(\pi(2H-3))]$, $\gamma_-=-1$ for \mathbf{Q} parallel to the ferromagnetic planes.

¹²A. Zheludev, *3-axis Resolution Library for Matlab*, <http://neutron.ornl.gov/~zhelud/reslib/> (2005).

¹³R. Maezono and N. Nagaosa, Phys. Rev. B **61**, 1189 (2000).

¹⁴A. J. Millis, Phys. Rev. B **55**, 6405 (1997).

¹⁵J. B. Goodenough, Phys. Rev. **100**, 564 (1955); J. Kanamori, J. Phys. Chem. Solids **10**, 87 (1959).

¹⁶*New Trends in the Characterization of CMR-Manganites and Related Materials*, edited by K. Baerner (Research Signpost, Trivandrum, 2005).

¹⁷H. Yoshizawa, H. Kawano, J. A. Fernandez-Baca, H. Kuwahara, and Y. Tokura, Phys. Rev. B **58**, R571 (1998).

¹⁸K. Hirota *et al.*, J. Phys. Soc. Jpn. **65**, 3736 (1996).

¹⁹A. Podlesnyak *et al.*, J. Phys.: Condens. Matter **6**, 4099 (1996).